
Proceedings Paper:
Kesserwani, G. orcid.org/0000-0003-1125-8384, Hajihassanpour, M., Pettersson, P. et al. (1 more author) (2024) What is the most efficient sampling-based uncertainty propagation method in flood modelling? In: Gourbesville, P. and Caignaert, G., (eds.) Advances in Hydroinformatics—SimHydro 2023 Volume 1 New Modelling Paradigms for Water Issues. SimHydro 2023, 08-10 Nov 2023, Chatou, France. Springer Water, 1 . Springer Nature Singapore , pp. 367-386. ISBN 9789819740710

https://doi.org/10.1007/978-981-97-4072-7_24

WHAT IS THE MOST EFFICIENT SAMPLING-BASED UNCERTAINTY PROPAGATION METHOD IN FLOOD MODELLING?

Georges Kesserwani[1], Mahya Hajihassanpour
Department of Civil and Structural Engineering, University of Sheffield, Mappin St, Sheffield City Centre, Sheffield, S1 3JD, UK
g.kesserwani@shef.ac.uk

Per Pettersson
NORCE Norwegian Research Centre, Nygårdsgaten 112, Bergen 5008, Norway
pepe@norceresearch.no

Vasilis Bellos

Laboratory of Ecological Engineering and Technology, Department of Environmental Engineering, Democritus University of Thrace, 67100 Xanthi, Greece
vbellos@env.duth.gr

KEY WORDS

Multiple uncertain variables, forward uncertainty propagation, flood extent and hazard rate, efficient histogram reproduction, probabilistic flood modelling

ABSTRACT

Modelling uncertainty propagation in flood modelling manifests in frequency of occurrence, or histograms, for quantities of interest, including the flood extent and hazard rating. Such modelling at the field-scale requires the identification of a more efficient alternative to the Standard Monte Carlo (SMC) method that can reproduce comparable output probability distributions with a reduced sample size. Latin Hypercube Sampling (LHS) is the most evaluated alternative but yields no considerable sample size reduction. Potentially better alternatives include Adaptive Stratified Sampling (ASS), Quasi Monte Carlo (QMC) and Haar-Wavelet Expansion (HWE), which are yet unevaluated for probabilistic flood modelling. In this paper, LHS, ASS, QMC and HWE are compared to quantify sample size reduction to reproduce output detailed histograms – for flood extent, and average and maximum hazard rating – while keeping the difference below 10 % to the reference SMC prediction. The comparison is done a synthetic test case with two (i.e., inflow discharge and Manning's coefficient) and three (i.e., further including the ground elevation) input random variables, and a real case with five input random variables. With two input random variables, all four alternatives yield sample size reductions, with QMC and HWE considerably outperforming the others; with three and more input random variables, HWE becomes inflexible and LHS underperforms. Still, QMC is a better choice than ASS to boost sample size reduction and should be preferred.

1. INTRODUCTION

Flood mapping uses a flood physical solver to estimate two-dimensional maps of flood-related quantities of interest, including the flood extent and/or the flood Hazard Rating (HR) [35, 44- 46]. Deterministic modelling does not account for the uncertainty inherent in the input variables, leading to suboptimal decisions in flood management and mitigation strategies [12]. Probabilistic flood modelling has become standard to propagate the uncertainty in the input random variables into the output probability distributions of quantities of interest. Such modelling can involve variability in multiple input variables,

[1] Corresponding author

non-smooth responses in any of the simulated quantities of interest, which may lead to complex probability distributions that are hard to capture such as those including multimodalities [2, 8, 42].

The present Uncertainty Quantification (UQ) framework assumes forward propagation of Type-B uncertainty, for which the variability in the random input parameters is generated from the means and standard deviations reported in published resources, and using an equiprobable uniform distribution [4]. Often, the forward propagation from such uncertain input variables into the probabilistically simulated quantities of interest is achieved using the Standard Monte Carlo method (referred herein to as SMC) [5, 13, 22, 24, 26, 39, 31, 48]. However, SMC requires a large sample size (N_s) to accurately propagate the uncertainty in the input parameters, which is not ideal for field-scale applications [2, 8]. This study aims to identify alternative-to-SMC UQ methods that use reduced N_s to reproduce $Flood\ extent$ and HR-related histograms in a maximum allowed difference of 10 %.

Existing studies are often limited to analyze the reduction in the N_s for one alternative to SMC often using the conventional statistical metrics like the mean or the variance [16, 46]. However, the use of conventional metrics may not be adequate to suggest reliable N_s reductions, because such metrics permit to overlook key information that could be present in complex output probability distributions (e.g., multimodal statistical peaks [2, 8, 41]. Hence, the reduction in the N_s for probabilistic flood modelling would be more reliable when using the more complex metric of the relative histogram difference. Among the few papers that explored this aspect, Beevers et al. [8] found that Latin Hypercube Sampling (LHS) [30] offers no reduction in N_s over SMC to reproduce $Flood\ extent$ histograms associated with D-dimensional uncertainty spaces including more-than-one random input variables ($D > 1$). The present UQ analysis framework is aimed to further assess other alternatives to SMC, which could better reduce N_s to reproduce the most uncertain quantity of interest among $Flood\ extent$ and HR-related histograms.

Accelerated Monte Carlo methods, or random sampling methods, rely on variance reduction to reduce N_s over SMC [23, 36]. From this category, LHS is a popular alternative [30, 38, 54, 56], but offer no reduction in N_s for $Flood\ extent$ histograms [2, 8]. Other random sampling techniques include the stratified sampling [11, 18, 38]. Stratified sampling and its Adaptive Stratified Sampling (ASS) versions [15, 37, 43] were shown to offer promising reductions in N_s over SMC for conventional statistical metrics: For synthetic fluid dynamics problems, ASS yielded 100-to-1000 times, 10-to-40 times, and 5-to-10 times smaller N_s with $D = 2$, 3 and 4, respectively [37], but is yet unassessed for flood modelling.

Deterministic realisation methods include Quasi Monte Carlo (QMC) and non-intrusive stochastic collocation approaches [53]. QMC [32, 51] uses low-discrepancy sequences of quasi-random samples for uncertainty spaces and using Hammersley sequences [20] reduce N_s by 40 times for D-dimensional spaces ($2 \leq D \leq 100$) [25, 50, 27]. In the non-intrusive stochastic collocation approach [6, 14, 55], global orthogonal polynomials are used as continuous basis functions to span the uncertainty spaces [42, 52]. However, this choice may not be suited for flood modelling to accurately represent multimodal discrete distributions [1, 42]. Using discrete basis functions of the Haar-Wavelet Expansion (HWE) [28] can remedies this issue, as exemplified by capturing critical physics of wetting and drying in the histograms using 4 times smaller N_s against SMC for a three-dimensional uncertainty space ($D = 3$) [42].

In this paper, LHS, ASS, QMC and HWE is compared to identify their potential N_s reduction against SMC to capture the histograms for $Flood\ extent$, average and maximum HR (HR_{ave} and HR_{max}). Section 2 describes the UQ analysis framework including details on: the generation of input variables (Section 2.1); the choice of the physical solver used for the probabilistic runs and definitions of $Flood\ extent$, HR_{ave} and HR_{max} (Section 2.2); the comparison approach based on the relative histogram difference against the reference SMC prediction (Section 2.3); and the definition and characteristics of flooding test cases for uncertainty spaces with $2 \leq D \leq 5$ (Section 2.4). In Section 3, the comparative analysis is presented to identify N_s^K, per alternative-to-SMC UQ method K (K = QMC, HWE, LHS and ASS), to keep a histogram difference below the target threshold of 7.5 % ± 2.5 %. Section 4 draws conclusions on the most efficient UQ method.

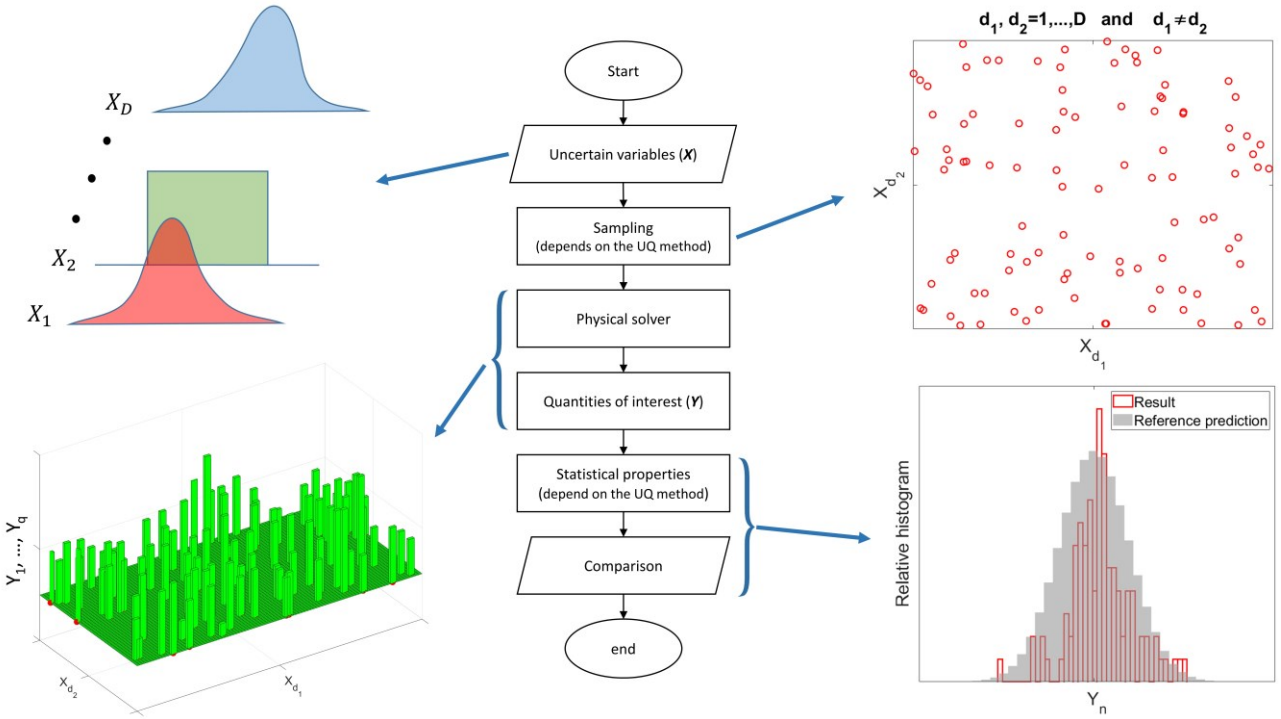

Figure 1: The UQ analysis framework. Upper-left: pre-defined uncertain variables, via probability distribution functions, spanning a *D*-dimensional uncertainty space; upper-right: a typical (random) sampling in the uncertainty space; lower-left: the output of a probabilistic run, after applying a physical solver for all samples, for the quantities of interest; lower-right: a relative histogram for a quantity of interest for evaluation against a reference prediction (brute-force SMC runs).

2. UQ ANALYSIS FRAMEWORK

The present uncertainty propagation framework is described in Fig. 1. The uncertainty in the values of the input parameters is represented by a vector of random variables, $\boldsymbol{X} = [X_1,...,X_D]$, in which each random variable is assigned a probability distribution that should reflect the information available about the corresponding input parameter (Fig. 1, upper left). It is commonly accepted that the choice of which probability distributions to adopt to model the uncertain hydrological parameters is less important than acquiring good estimates of their means and standard deviations. Therefore, the input random variables are generated based on given means and standard deviations from surveyed uncertainty ranges in published resources, and using uniform, or rectangular, probability distributions to conservatively model Type-B uncertainty (i.e., with equal probabilities) [4]. The input random variables $\boldsymbol{X}$ are sampled, with either a random sampling (e.g., Fig. 1, upper-right) or deterministic sampling, depending on the UQ method. A probabilistic run is achieved by applying a physical solver to all the samples (N_s simulations), leading to output samples for selected quantities of interest $\boldsymbol{Y} = [Y_1,...,Y_q]$ (Fig. 1, lower-left). Histogram(s) for $\boldsymbol{Y}$ are generated for each UQ method, normalised to N_s to become relative histogram(s), to assess N_s reduction such that to keep the difference against the reference prediction (Fig. 1, lower-right) below the target threshold of 7.5 % ± 2.5 %.

2.1 Generation of the input random variables

In probabilistic flood modelling, the three most significant uncertain variables are the inflow discharge, Manning coefficient, and ground elevation [3, 9, 24]. Here, each uncertain (i.e., random input) variable is assumed to result from the same measurement error at any point in time for the inflow discharge(s) and at any point in space for the Manning coefficient and the ground elevation. With this assumption, the dimensionality of the uncertainty space is the number of input variables for computational feasibility. Otherwise, non-correlated, cell-wise variations in the ground elevation would need a distinct random variable for every cell, leading to an unfeasible increase in the dimensionality [47]. The uncertainty in each mean inflow discharge, $\bar{Q}(t)$ at a time instant t, is often assigned to a 16 % range [7]. Therefore, a uniform inflow discharge random variable, $Q(t, \xi_Q)$, follows:

$$Q(t,\xi_Q) = \bar{Q}(t) + \xi_Q\ \sigma_Q(t) \tag{1}$$

where ξ_Q is a random variable taking values in $[-1,+1]$ and $\sigma_Q(t) = 0.08\bar{Q}(t)$ is the range of variation with respect to the mean $\bar{Q}(t)$. For P mean inflow discharges, $\overline{Q_1}(t)$, …, $\overline{Q_P}(t)$ ($P > 1$), the variation in each of $Q_1(t,\xi_{Q_1})$, …, $Q_P(t,\xi_{Q_P})$ follows Eq. (1), assuming that ξ_{Q_1}, …, ξ_{Q_P} are not intercorrelated [*Neal et al.*, 2013], leading to an uncertainty space dimension of $D = P$.

The Manning coefficient's uncertainty depends on friction elements (e.g., vegetation, land, or soil type) and is often assigned a range of 10 %, from bibliographical values and calibration to match observed flood-related data [10, 33]. Thus, the uniform Manning coefficient random variable follows:

$$n(\xi_n) = \bar{n} + \xi_n\ \sigma_n \tag{2}$$

where ξ_n is a random variable taking values in $[-1,+1]$, $\bar{n}$ is a given mean constant Manning coefficient and $\sigma_n = 0.05\ \bar{n}$ is the range of variation with respect to $\bar{n}$. It is sometimes necessary to also include uncertainty in the mean ground elevation variable, $\bar{z}(x,y)$, with respect to which the range of variation $\sigma_z(x,y)$ can be generated from the analysis of the Digital Elevation Model (DEM) data. The range of variation $\sigma_z(x,y)$ is often assigned a measurement error uncertainty as high as 10 % depending on the quality of the DEM data. Hence, the uncertainty in $\bar{z}(x,y)$ may be significant in some locations, informed by local estimates of $\sigma_z(x,y)$. Hu et al. [21] and Liu et al. [29] estimated $\sigma_z(x,y)$ for LiDAR-based DEMs as a function of the diagonal length of the DEM's cell size, denoted by l_d, and the local curvature for the DEM's value at this cell, denoted by $M(x,y)$. Their estimates suggest significant $\sigma_z(x,y)$ either when the DEM resolution is coarse or when the DEM's cells represent a topographic area with large curvatures (e.g., riverbanks or buildings). As these estimates for $\sigma_z(x,y)$ have different weights for $M(x,y)l_d^2$ to analyze distinct DEM data types, $\sigma_z(x,y)$ can generally be estimated to $|c\ M(x,y)l_d^2|$, where c is a user-defined weight identified by a DEM-specific sensitivity analysis, suggesting c around 0.04 to 0.125 for realistic, uneven DEM, and 5 for idealistic, smooth DEM. After estimating $\sigma_z(x,y)$, the ground elevation random variable, for ξ_z varying in $[-1,+1]$, follows:

$$z(x,y,\xi_z) = \bar{z}(x,y) + \xi_z\ \sigma_z(x,y) \tag{3}$$

2.2 Physical solver and quantities of interest

For a selected UQ method at a fixed N_s, a physical solver should be employed to make a probabilistic run, or ensemble of N_s simulations, to propagate the variations in the input variables (Eqs. 1-3) into output probability distributions. The first-order finite volume hydrodynamic solver of the LISFLOOD-FP suite was employed, using the version parallelized on Graphical Processing Units (GPU), so-called GPU-FV1 [19]. The probabilistic run leads to output samples for the water depth, $h(x,y,t)$ and velocity field magnitude, $V(x,y,t)$, that are post-processed into the following quantities of interest:

- ***Flood extent.*** It is the sum of the area of the computational cells with non-zero water depth h , i.e., total wet area. The $Flood\ extent$ has often been used in probabilistic flood modelling to analyse flood extent frequencies [2, 8].
- ***Average Hazard Rate*** ($\boldsymbol{HR_{ave}}$) ***and maximum Hazard Rate*** ($\boldsymbol{HR_{max}}$). The flood HR is defined as: $HR = h \times (V + 0.5)$; and, it has been used to provide more information on velocity impacts to assets including structural damage to residential buildings, damages to road infrastructures, and risks to people's life and injury [44]. In this study, HR_{ave} and HR_{max} quantify the average and maximum flood HR over the computational area.
- ***Flood timing.*** The above quantities are evaluated at $flood\ timing$, t, of maximum flood extent.

2.3 Comparison approach using the relative histogram difference

In SMC the order of convergence is inversely proportional to $N_s^{1/2}$, requiring a large N_s to reproduce a true reference prediction (e.g., known analytical functions [27]). Four selected alternative-to-SMC UQ methods are compared to potentially reduce N_s while keeping a relative histogram difference below 10 % against the reference SMC prediction for the most relevant quantity of interest. The alternatives

are HWE and QMC, from the deterministic realisation methods, and ASS and LHS from the random sampling methods. Compared to the conventional statistics like the mean or the variance, a histogram can inform on key aspects contributing to the overall statistics, such as multimodalities in a frequency of occurrence, which can otherwise be missed (i.e., as shown in [41]).

For a quantity of interest, among $Flood\ extent$, HR_{ave} and HR_{max}, the relative histogram predicted by the UQ method K for a fixed N_s^K (K = SMC, QMC, HWE, LHS and ASS) is compared to the relative histogram of the reference prediction–produced using SMC with a N_s that is 2.5-to-320 times larger than N_s^K, depending on the affordability of SMC per test case to make the probabilistic run (i.e., to produce the reference prediction). Comparing the difference between these two relative histograms may not be straightforward. On the one hand, a relative histogram is sensitive to the number of bins, N_{bins}, as too wide bins can overlook multimodalities. As a rule of thumb, N_{bins} depends on the N_s^K, which here ranges between 125 and 4096. For this range of N_s^K, N_{bins} can be as large as 40 to analyze flood extent frequency occurrence [8]. Therefore, the three values for N_{bins} = {10, 20, 40} are considered when comparing the difference between these two relative histograms. On the other hand, for a fixed N_{bins}, comparing two relative histograms, can either be bin-wise or via a cross-bin approach [40]. The bin-wise approach measures the difference bin-by-bin, and the cross-bin approach also incorporates the correlations from the differences at the neighbouring bins. Although less sensitive to N_{bins}, the cross-bin approach tends to predict zero differences in regions of uniform frequency distributions [40]. Hence, the bin-wise approach is used to compare the two histograms, as follows [49]:

$$Relative\ histogram\ difference\ (\%) = 100 \times \sum_{j=1}^{N_{bins}} \left| f_{ref_j} - f_j \right| \tag{4}$$

In Eq. (4), f_j and f_{ref_j} denote the relative frequency (normalised by N_s^K) inside the j^{th} bin for the histogram predicted by the selected UQ method and for the histogram of the reference prediction, respectively. The identified N_s^K per alternative-to-SMC UQ method K (K = QMC, HWE, LHS and ASS) are then used to quantify the reduction in terms of the following relative-to-SMC speedup ratio:

$$Speedup\ ratio\ = N_s^{SMC}/N_s^K (\text{K = QMC, HWE, LHS and ASS}) \tag{5}$$

Note that, the quantified speedup ratios (Eq. 5) for the identified N_s^K are only based on the relative histogram difference (Eq. 4); in other words, not based on the standard errors of the mean and the variance, which lead to greatly larger speedup ratios, and that the identified N_s^K required 60 times more runs, or replications, per random sampling method (i.e., SMC, ASS and LHS) [19].

2.4 Definition and characteristics of the test cases

Two probabilistic flood modelling test cases are used to assess the alternative-to-SMC UQ methods K (K = QMC, HWE, LHS and ASS) to potentially reduce N_s^K over N_s^{SMC} to keep a maximum threshold of 10 % for the relative histogram difference (Eq. 4), while also analyzing the effect of N_{bins} = {10, 20, 40}. The first test case is a synthetic "Rapidly propagating flood over a smooth terrain" (Section 2.4.1). It is employed to identify N_s^K for two sub-cases: D = 2 for the two input random variables: $Q(t, \xi_Q)$ and $n(\xi_n)$; and, D = 3 for the three input random variables: $Q(t, \xi_Q)$, $n(\xi_n)$ and $z(x, y, \xi_z)$. The aim is to identify the N_s^K that keeps the relative histogram difference (Eq. 4) below the average target threshold of 7.5 % for all the quantities of interest, and then accordingly quantify the speedup ratios (Eq. 5). The second test case assesses the validity of the best two selected candidates among the random sampling methods and the deterministic realization methods (QMC and ASS) for probabilistic modelling of the "Carlisle 2005 flooding" (Section 2.4.2). This test case is featured by a D = 5 including three input random discharge variables, $Q_p(t, \xi_{Q_p})_{p=1,2,3}$, and the input random variables for the Manning coefficient and the ground elevation, $n(\xi_n)$ and $z(x, y, \xi_z)$ for two choices of N_s^K identified in the previous test case.

2.4.1. Rapidly propagating flood over a smooth terrain

In this synthetic test case [34], the mean inflow discharge, $\bar{Q}(t)$, is 65.5 $m^3 s^{-1}$. The inflow discharge variable $Q(t, \xi_Q)$ enters from the left boundary into a small domain area of 0.3 km × 0.1 km that has a mean Manning coefficient $\bar{n}$ = 0.01 with variation of $n(\xi_Q)$. The mean ground elevation variable $\bar{z}(x, y)$ is taken from a pseudo-two-dimensional DEM at 2 m resolution and its variation $z(x, y, \xi_z)$ is estimated for $\sigma_z(x, y)$, using c = 5. The flood timing is 193 seconds, when a simulation stops for analysis of $Flood\ extent$, HR_{ave} and HR_{max}. Using 7,500 computational cells, a single simulation took 3 seconds and the probabilistic SMC run used N_s = 40,000 to produce the reference prediction.

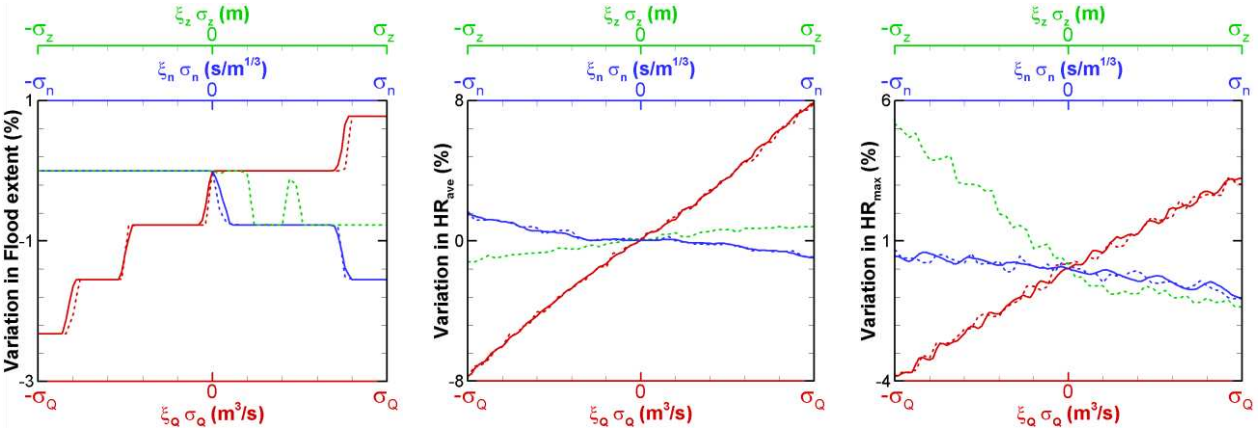

Figure 2: Rapidly propagating flood over a smooth terrain. Centreline plots of the projections from the D-dimensional response surfaces for $Flood\ extent$, HR_{ave} and HR_{max}, showing their variations in each uncertainty dimension for the case with D = 2 (solid lines) and the case with D = 3 (dotted lines).

From the reference prediction, D-dimensional response surfaces for each of $Flood\ extent$, HR_{ave} and HR_{max} can be produced to analyse how the variations in the input variables (from their mean values) propagate into each of the quantities of interest. Figure 2 shows the plots of the centreline projections of the response surfaces of each random variable for the sub-cases with D = 2 (solid lines) and with D = 3 (dotted lines). With D = 2, larger variations are seen due to the inflow discharge variable compared to variations due to the Manning coefficient variable. For $Flood\ extent$, the variations due to these two variables are few, flat states connected by steep jumps, that are more frequent for the inflow discharge variable. For HR_{ave}, the variations are quite linear; but the variation due to the inflow discharge variable is steeper and far more deviates from the close-to-flat variation due to the Manning coefficient variable. For HR_{max}, though the variations have a lower range of variability, they display non-smooth waviness compared to HR_{ave}. Its lower range of variability arise from the fact that $Flood\ timing$ is closer to the time when the maximum of HR_{ave} is reached, than to the time when HR_{max} reaches its maximum. With D = 3, the variations in both dimensions of the inflow discharge variable and the Manning coefficient remain quite unchanged for all the quantities of interest. In the ground elevation variable, the variations for $Flood\ extent$ and HR_{ave} are close to zero, thus relatively insignificant, which is in contrast with the variation for HR_{max} that is noticeably large, significantly adding up to the overall HR_{max} variation. Overall, the analysis of Figure 2 shows that HR_{max} is the most uncertain quantity of interest in this test, in which the responses for $Flood\ extent$ and HR_{ave} are similar with D = 2 and 3.

A range of choices to select N_s^K per UQ method is explores to include 500 samples per uncertain input variable as recommended in [8]. For HWE, the range of N_s^{HWE} = {64, 256 ,1024, 4096} is used with D = 2 and of N_s^{HWE} = {64, 512, 4096} with D = 3 [42]. The other UQ methods (SMC, LHS, ASS and QMC) can be given the same range of N_s^K ={125, 250, 500, 1000, 2000, 4000}. In Section 3.1, the identified N_s^K that keep the relative histogram difference below the average threshold of 7.5 % are discussed, together with quantifications of their relative-to-SMC speedup ratios and analysis of their sampling patterns in the uncertainty space and ability to reproduce different shapes of relative histograms.

2.4.2. Carlisle 2005 flooding

This test case [17] is also adjusted to become probabilistically impacted by five input random variables. The fluvial flooding is driven by three given mean inflow discharge variables, $\bar{Q}_p(t)_{p=1,2,3}$, originating

from rivers Eden, Caldew and Petteril, with the variations of their random variables, $Q_p(t, \xi_{Q_p})_{p=1,2,3}$, shown in Figure 3a-c. The inflow drivers lead to a flood propagation over a 14.5 km^2 area in the city of Carlisle, where the mean Manning coefficient is often considered to be a constant of $\bar{n}$ = 0.055, based on which the random input variable $n(\xi_n)$ is introduced. The mean ground elevation variable, $\bar{z}(x, y)$, is based on a 5 m resolution DEM (finest available), and its random input variable $z(x, y, \xi_z)$ was based on estimates for $\sigma_z(x, y)$ using c = 0.04, taking the values (Figure 3d).

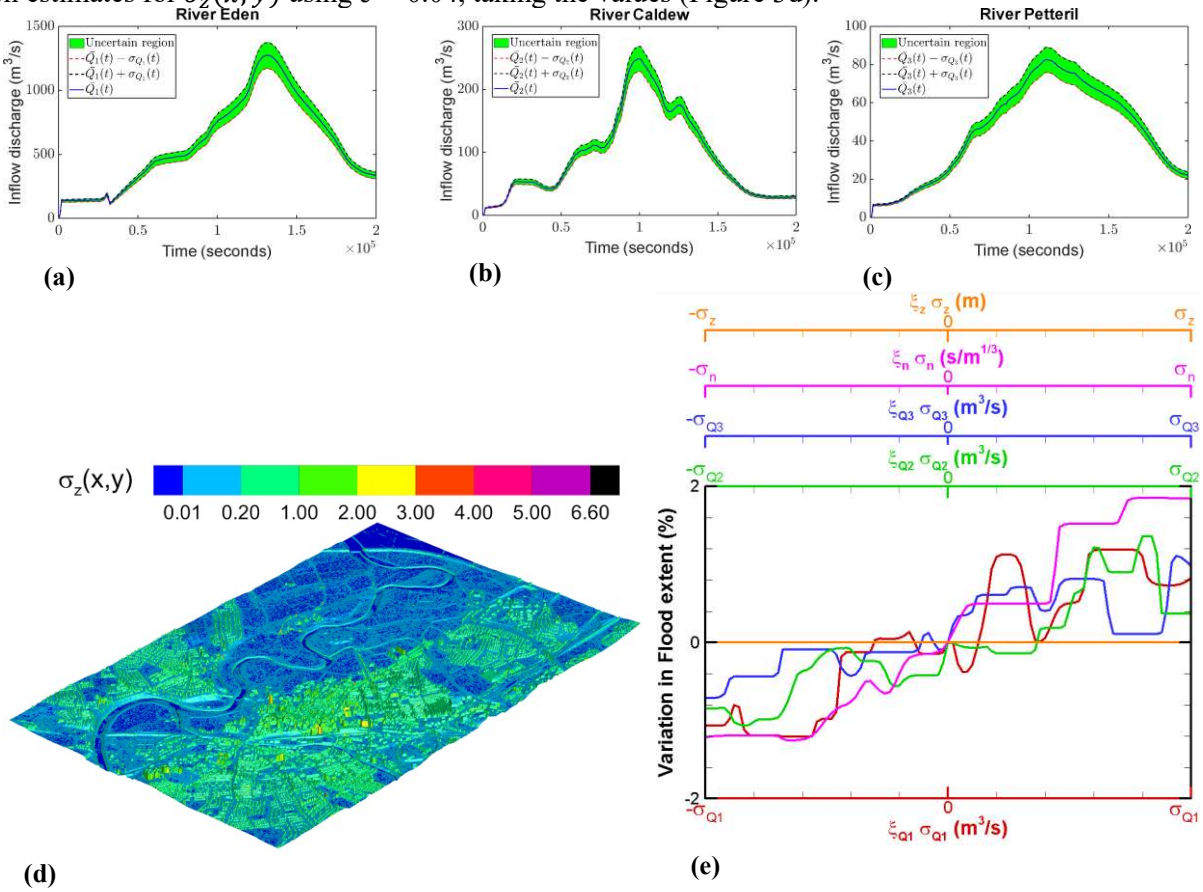

Figure 3: Carlisle 2005 flooding. Subfigure (a) to (c) show the variation in inflow discharge originating from rivers Eden, Caldew, and Petteril, respectively; subfigure (d) shows the variation from the mean ground elevation variable; and subfigure (e) shows the centreline plots of the projections from the response surface into each uncertainty dimension.

A single simulation used 581,061 cells and was stopped at the flood time of 40 hours, costing a runtime of 400 seconds. This results in a large, elapsed, runtime to make a probabilistic SMC run, limiting the reference prediction to N_s = 10,000. Here, $Flood\ extent$ is the most uncertain quantity of interest to investigate, as is usually the case with such a slowly propagating flood over rough and realistic terrains [2, 8, 19]. Hence, only the 5-dimensional response surface for $Flood\ extent$ is produced from the reference prediction to analyze its variation due to each of the five random variables – again via the plots of centreline projections included in Figure 3e. The strongest, largest, and widest range of variation in the response surface arises due to the Manning coefficient variable. The range of variation due to each of three inflow discharge variables is comparatively weaker, but a cumulative variations is expected to lead to an overall stronger variation than that due to the Manning coefficient variable. For any of these four random variables, the type of variation for $Flood\ extent$ is quite similar, exhibiting semi-flat states in some regions or non-smooth patterns in other regions, which are connected by steep jumps. Comparatively, a flat variation is observed due to the ground elevation variable, suggesting that this variation would insignificantly influence the predictions compared to any other variation. This finding suggests giving less importance to the variation in the ground elevation variable for probabilistic modelling over real and highly rough topologies. In Section 3.2, only ASS and QMC are compared using N_s^K = 2000 and 4000 (justified in Section 3.1), with validation to reproducing the relative histogram for the $Flood\ extent$ quantity.

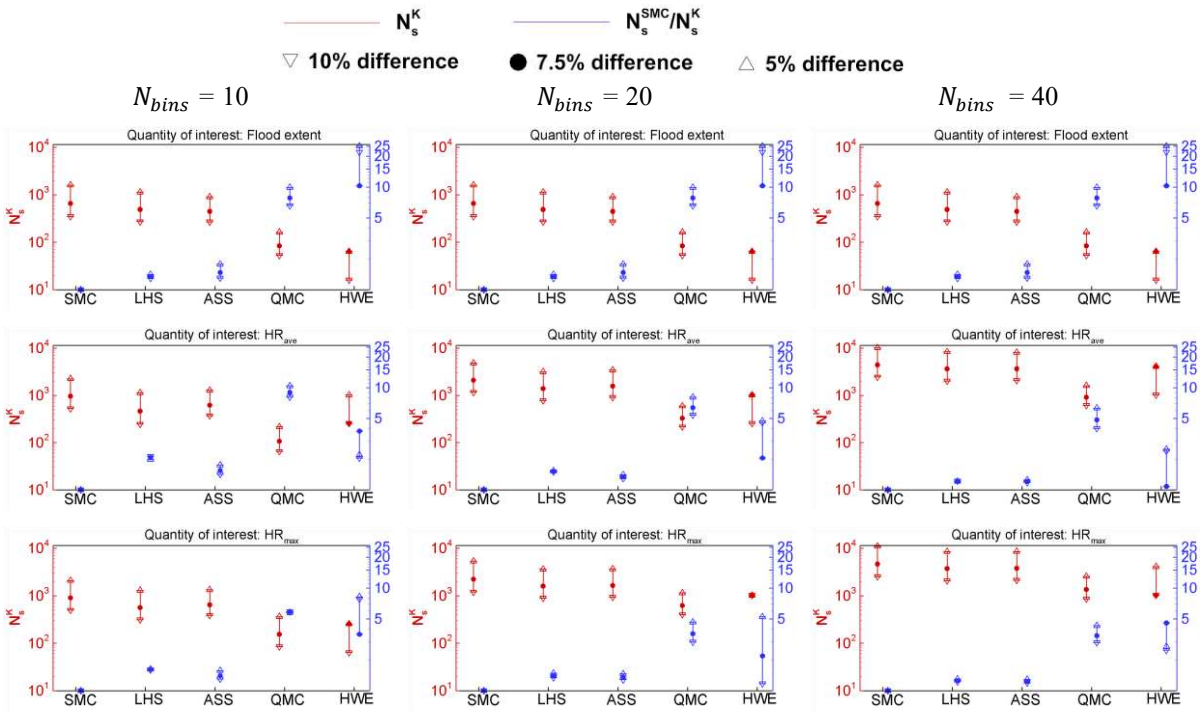

Figure 4: Rapidly propagating flood over a smooth terrain. The N_s^K and relative-to-SMC speedup ratio (Eq. 5) to meet the target difference of 7.5 % ± 2.5 % for $Flood\ extent$ (upper panel), HR_{ave} (middle panel), and HR_{max} (lower panel), using N_{bins} = {10, 20, 40} (left to right).

3. RESULTS AND DISCUSSION

3.1 Rapidly propagating flood over a smooth terrain

3.1.1. Sub-case with D = 2

Figure 4 shows the identified N_s^K and relative-to-SMC speedup ratios N_s^{SMC}/N_s^K to keep the target average threshold for N_{bins} = {10, 20, 40}. All the UQ methods achieve speedup ratios greater than one, thus lead to identifying N_s^K that offer a reduction over N_s^{SMC}. However, the reduction differs depending on the quantity of interest. $Flood\ extent$, since it has few flat variations in its responses, leads to the smallest N_s^K alongside the highest speedup ratios and irrespective of N_{bins}. The identified N_s^{LHS} and N_s^{ASS} are at least one order of magnitude larger than N_s^{QMC} and N_s^{HWE}, yielding speedup ratios that range between 1.1 and 1.8 for LHS and ASS and between 5 and 25 for QMC and HWE. For HR_{ave} and HR_{max}, the identified N_s^K are expectedly larger, up to one order of magnitude with the largest N_{bins} = 40. This leads to a drop in the lower bound of the speedup ratios for QMC and HWE from around 5 to around 1.1. However, this drop occurs due to the overly large $N_s^{HWE} = 4096$ identified for HR_{ave}. With the lower $N_s^{HWE} = 1024$, the relative histogram difference for $Flood\ Extent$ and $HR_{\max}$ are 1.3 % and 6.4 %, respectively; however, the difference for HR_{ave} becomes 8.1 %, which is not below the average target difference of 7.5 %. The only next possible choice for an N_s^{HWE} that is larger than 1024, is $N_s^{HWE} = 4096$, given the inflexibility of HWE in the selection of N_s^{HWE}, which is four-times larger leading to a difference of 3.8 % for HR_{ave} that is below the target average difference of 7.5 %. Therefore, QMC is a better alternative since its lower bound remains around four-times higher than 1.1. The speedup ratios for LHS and ASS remain similar to the ratios identified for $Flood\ extent$, subject to a slightly lower upper bound, of 1.30. For each UQ method for the largest N_s^K was identified to meet the average threshold difference of 7.5 % for the most uncertain quantities of interest with N_{bins}= 40. The sampling with SMC needed $N_s^{SMC} = 4675$ and a more efficient sampling is achieved by LHS, with 937 fewer samples ($N_s^{LHS} = 3738$). ASS performs like LHS, needing slightly more samples ($N_s^{ASS} = 3790$). HWE leads to overtly refined sampling ($N_s^{HWE} = 4096$), caused by its inflexibility. QMC achieves the highest reduction ($N_s^{QMC} = 1359$) and is thus the most efficient sampling of the uncertainty space with D = 2.

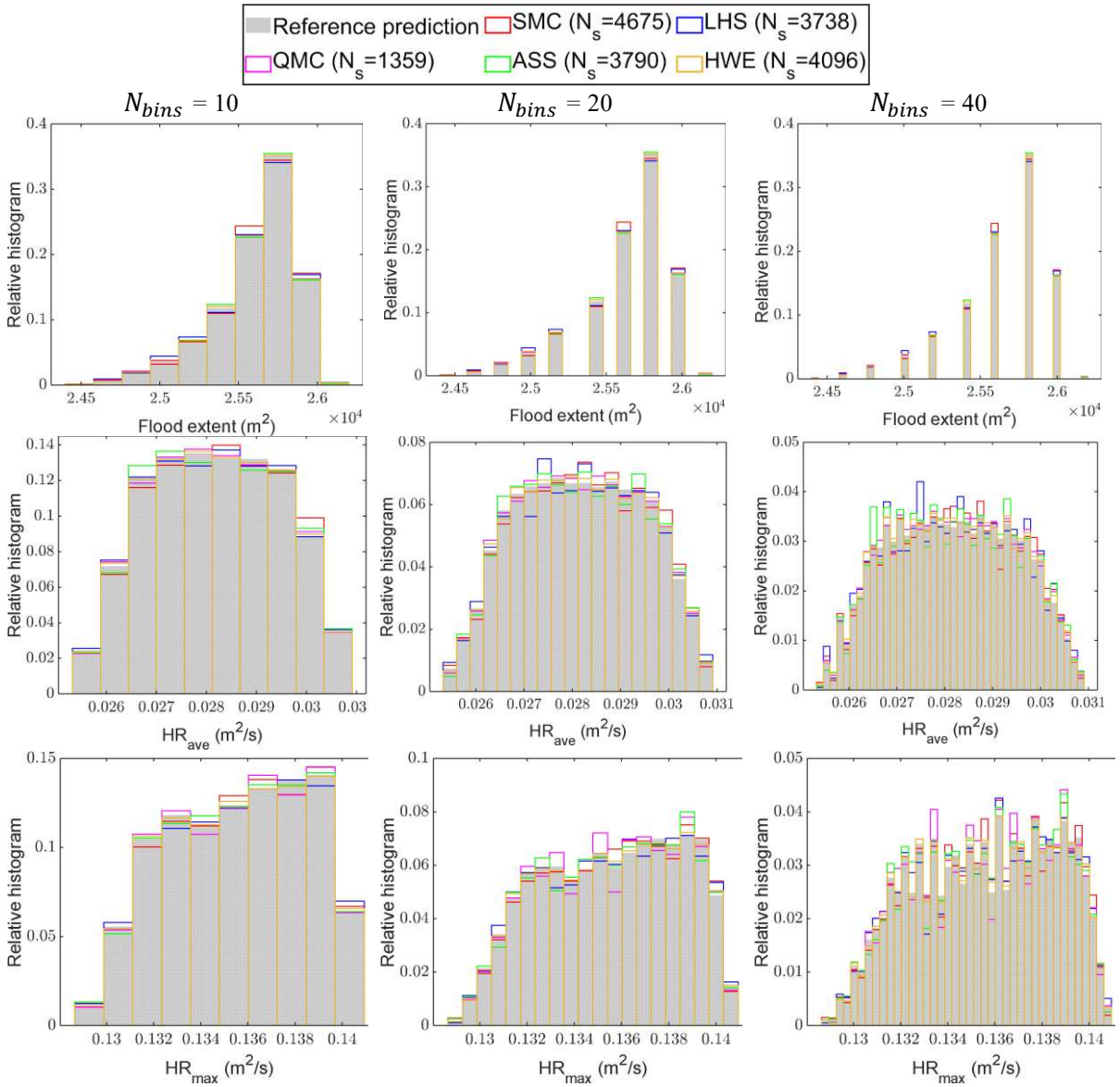

Figure 5: Rapidly propagating flood over a smooth terrain. Relative histogram plot per UQ method for the N_s^K. The plots for the coarser relative histograms using N_{bins} = {10, 20} are based on the same N_s^K.

Figure 5 shows the plots of the relative histograms for $Flood\ extent$, HR_{ave} and HR_{max}, extracted per UQ method for the identified N_s^K based on N_{bins} = 40 (shown in Fig. 9), and in which the coarser relative histograms using N_{bins} = {10, 20} are based on the same N_s^K. For $Flood\ extent$, the relative histograms exhibit a discrete distribution for N_{bins} = {20, 40}, which tends to look like a left-skewed unimodal distribution with the coarsest N_{bins} = 10, suggesting that larger N_{bins} is still needed despite the few discrete states in this quantity of interest. For HR_{ave}, the relative histograms follow an almost symmetric distribution that becomes more complex with larger N_{bins}. The relative histograms seen for HR_{max} are the most complex overall, in particular as N_{bins} is enlarged to 40 leading to a quite irregular distribution. Among the histogram distributions, the discrete one is the most accurately captured by all the UQ methods. The symmetric distribution seems to be more challenging to capture, though it is better reproduced with the deterministic realisation methods (QMC and HWE) than with the random sampling methods (SMC, LHS and ASS). The distribution for HR_{max}, involving multimodalities, is the most challenging to capture for which all the UQ methods reach the average threshold difference of 7.5 %.

3.1.2. Sub-case with D = 3

Here, the analysis is restricted to HR_{max} as it is the only quantity of interest that changes drastically as D is increased to 3 – compared to $Flood\ extent$ and HR_{ave} that retain similar responses to as with D =

2. Figure 6a shows the N_s^K identified per UQ method and their relative-to-SMC speedup ratios N_s^{SMC}/N_s^K to keep the target threshold difference with N_{bin} = {10, 20, 40}. As can be observed, there is no notable reduction in the identified N_s^{LHS} and N_s^{ASS} since they lead to a speedup ratio range close to 1. The identified N_s^{QMC} and N_s^{HWE} yield a speedup ratio range of around 0.5-to-2.0. These upper and lower bounds are, however, fluctuations reached by HWE, which leads to an average speedup ratio that is lower than the average speedup ratio of 1.6, which is consistently preserved by QMC. This suggests that QMC is a better choice to meet the average threshold difference of 7.5 % while having N_s somewhere between 2000 and 4000.

Figure 6b shows the plots of the relative histograms for HR_{max}, shown for each UQ method for the identified N_s^K to meet the average threshold difference of 7.5 %, based on N_{bins} = 40. The relative histograms follow a triangular distribution that displays sharper details as N_{bins} is enlarged, making it even more challenging to capture by the UQ methods *K* with a N_s^K between around 2000 and 4000 (*K* = SMC, LHS, ASS and QMC). QMC again outperforms the other methods with a relatively smaller N_s^{QMC}= 2400, that is closer to the lower bound of 2000, compared to any other UQ method *K* that yield a N_s^K that is closer to the upper bound of 4000.

Overall, the alternative-to-SMC UQ methods with the identified N_s^K (Section 3.1) leads to predictions that are close to the average threshold difference of 7.5 % without exceeding the maximum threshold of 10 %. Among these methods, QMC and ASS keep the relative histogram prediction to 7.5 % and tend to perform better as *D* is increased, with N_s^{ASS} and N_s^{QMC} remaining within 2000 and 4000. Therefore, ASS and SMC are investigated further for the real case study involving five input random variables (*D* = 5) to only analyze their $Flood\ extent$ histograms (Section 3.2) using N_s^K = {2000, 4000}.

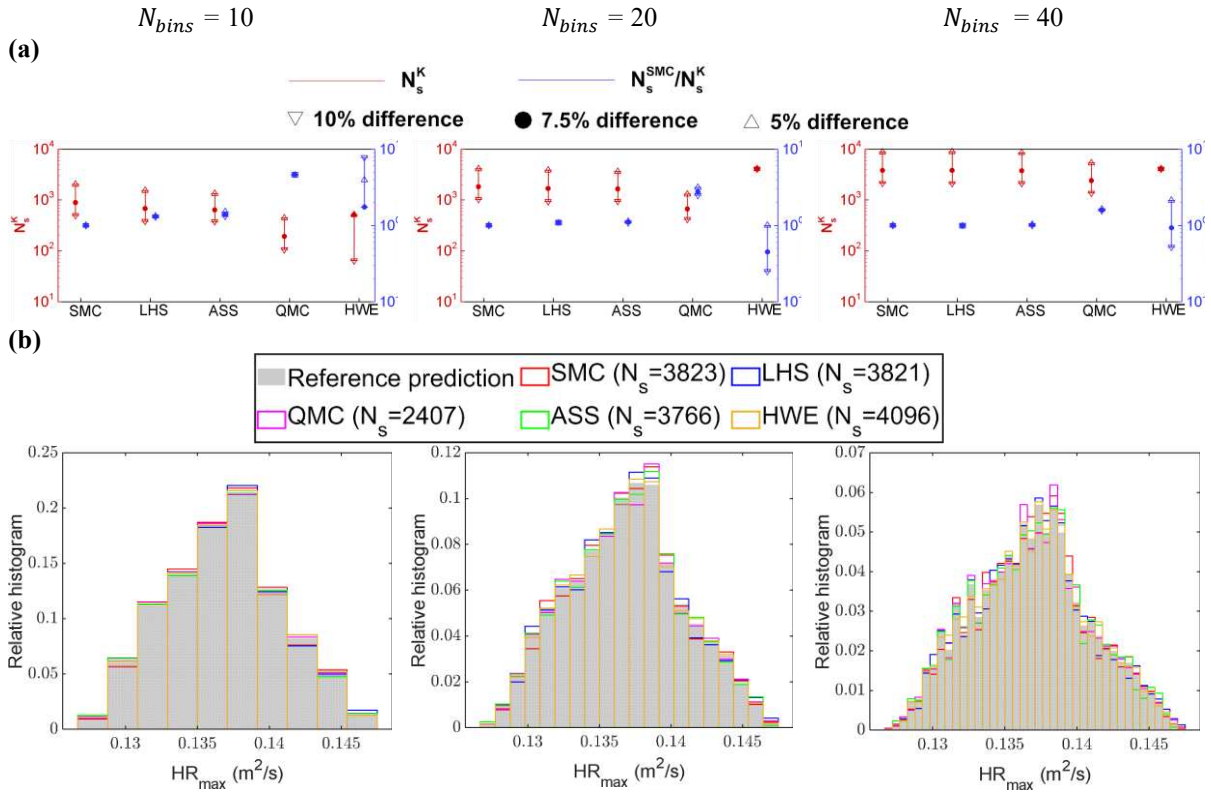

Figure 6. Rapidly propagating flood over a smooth terrain. (a) The N_s^K and relative-to-SMC speedup ratio (Eq. 5) to meet the target difference of 7.5 % ± 2.5 % for $Flood\ extent$ (upper panel), HR_{ave} (middle panel), and HR_{max} (lower panel), using N_{bins} = {10, 20, 40} (left to right); and (b) Relative histogram plot per UQ method for the N_s^K identified to keep the target average difference of 7.5 % based on N_{bins} = 40.

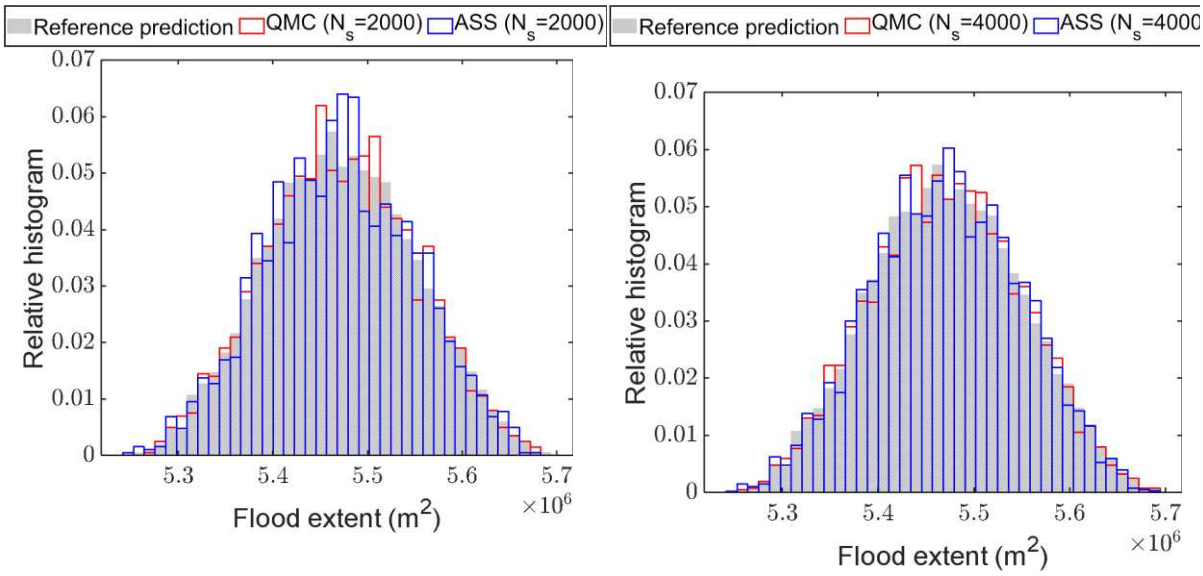

Figure 7: Carlisle 2005 flooding. Relative *Flood extent* histograms (using N_{bins} = 40) per UQ method K (K = QMC and ASS) for N_s^K = 2000 (left) and 4000 (right).

Table 1. Carlisle 2005 flooding. Relative histogram differences (via Eq. 4) for *Flood extent* against the test-specific reference prediction considering N_{bins} = {10, 20, 40} for the UQ methods K (K = QMC and ASS).

N_{bins}	Relative histogram difference (%)			
	$N_s = 2000$		$N_s = 4000$	
	ASS	QMC	ASS	QMC
10	4.1	2.6	2.4	4.4
20	8.7	5.1	6.1	6.2
40	12.5	8.6	8.5	7.7

3.2 Carlisle 2005 flooding

In Figure 7, the relative *Flood extent* histograms predicted by QMC and ASS are compared to the reference prediction for N_s^K = 2000 (left) and 4000 (right). The histograms follow a symmetric distribution that is better captured by QMC compared to ASS. Table 1 shows the relative histogram differences against the test-specific reference prediction for QMC and ASS for N_{bins} = {10, 20, 40} and N_s^K = {2000, 4000}. For N_s^K = 2000, the relative histogram difference increases with both QMC and ASS with larger N_{bins}, but the difference with ASS increases at faster rate than the difference with QMC, leading to differences around 8.6 % and 12.5 % for the largest N_{bins} = 40, respectively. This suggests favouring QMC over ASS when using a N_s^K close to 2000. For N_s^K = 4000, the relative histogram difference with ASS is lower than that with QMC for N_{bins}= 10, almost identical for N_{bins}= 20 but slightly higher for N_{bins}= 40, suggesting that the increase in N_{bins} may be of less influence as N_s^K is close to 4000. Overall, QMC leads to a difference that is closer to the average threshold difference of 7.5 %, with both N_s^{QMC} = 2000 and 4000, and irrespective of N_{bins}; whereas ASS only meets this criterion with N_s^{ASS} = 4000. This means that to keep the relative histogram difference below the maximum threshold of 10 %, using N_s^{QMC} = 2000 is feasible to achieve a relative-to-SMC speedup ratio of 5 with QMC, for this test case, whereas only a speedup ratio of 2.5 can be achieved with ASS by using N_s^{ASS} = 4000.

4. CONCLUSIONS

Four uncertainty quantification methods were assessed to find alternatives to the Standard Monte Carlo (SMC) method for reproducing flood-related histograms, efficiently at a reduced sample size: two based on random sampling, which are Latin Hypercube Sampling (LHS) and Adaptive Stratified Sampling (ASS), and two based on deterministic realisation, which are Quasi Monte Carlo (QMC) and Haar-Wavelet Expansion (HWE). The reproduced flood-related histograms were evaluated for three quantities

of interest, the $Flood\ extent$ and the average and maximum hazard rating (HR_{ave} and HR_{max}). These quantities stemmed from the probabilistic modelling of torrential and fluvial floodplain flows, impacted by uncertainty from at least two input random variables amongst the inflow discharge(s), the Manning coefficient and the ground elevation. The relative histograms predicted by each of the four alternative-to-SMC methods were validated against the reference SMC prediction achieved by brute-force probabilistic runs using a much larger sample size.

Firstly, the four methods were exhaustively compared for a synthetic rapidly propagating flood over a smooth terrain to include diagnostic analyses of their sample size reduction for two sub-cases: one with two input random variables for the inflow discharge and the Manning coefficient; and, the other with three input random variables, further incorporating the input random variable for the ground elevation. The analyses identified a sample size between 2000 and 4000 for the four methods to keep the relative histogram difference below an average threshold around 7.5 % with respect to the reference prediction. The identified sample sizes were mostly based on HR_{max}, since it was the most uncertain quantity of interest, exhibiting the highest level of non-smoothness in the responses, and on the largest number of bins, of 40, since using fewer bins led to better sample size reductions. With two input random variables, the sample size for LHS was slightly smaller than that for ASS, both yielding about 900 samples less than the sample size predicted for SMC, or a relative-to-SMC speedup ratio in the range of 1.2-to-1.8. However, LHS and ASS yielded no considerable speedup ratios with three input random variables; despite this, the sample size for ASS became smaller than that of LHS, suggesting a tendency for ASS to potentially outperform if the number of input random variables is increased beyond three. QMC and HWE yield higher speedup ratios, in range of 1.1-to-25, with two input random variables; the lower bound of 1.1 was caused by the inflexibility of HWE to use any sample size between 1024 and 4096, as opposed to QMC that had a four-times higher lower bound. With three input random variables, the speedup ratios for QMC and HWE dropped, to a range of 0.5-to-2.0, though QMC preserved an average speed up ratio of 1.6; again, the lower and upper bounds were fluctuations arising from the (aforementioned) inflexibility of HWE. Common to both sub-cases, QMC entailed a sample size closer to 2000, compared to the sample size for LHS, ASS and HWE that were closer to 4000.

Secondly, therefore, ASS and QMC were validated using sample sizes of 2000 and 4000 to reproduce the reference prediction for the $Flood\ extent$, which is the most uncertain quantity of interest for this real-world fluvial flooding scenario with five input random variables. For the sample size of 2000, both ASS and QMC capture the reference $Flood\ extent$ histogram, with a difference below the maximum threshold of 10 %, with low number of bins, of 10 and 20; however, ASS failed to meet this threshold when the number of bins is enlarged to 40. For the larger sample size of 4000, ASS and QMC predicted relative histogram differences that meet the maximum threshold, irrespective of the number of bins, suggesting that they are both valid choices for sample sizes as large as 4000 to get a speedup ratio of 2.5. However, only QMC could meet this threshold to further reduce the sample size somewhere close to 2000 and boost the speedup ratio to 5.

Overall, the comparative analyses in this study identify QMC to be the simplest and most efficient alternative-to-SMC for probabilistic flood modelling applications, including rapid and slow flows, driven by more than one input random variable but not exceeding five. The speedup ratio for QMC is in the range of 1.6-to-5. However, this ratio has been quantified for suboptimal conditions (i.e., for the relative histogram metric in order to capture the full details of the probability distributions, for the most uncertain flood-related quantity of interest and the largest number of bins); thus should be larger when using less sensitive metrics (e.g., the standard errors of the mean and variance) or when targeting a flood-related quantity with low and/or smooth variations in its responses. Despite the limitations of this study, its findings still provide useful insights into the potential utility of QMC to speedup probabilistic modelling of more sophisticated water resource problems including more than five random variables such as, for example, to use QMC with a multi-physics solver to support a data-driven model to minimize the number of sub-samples of the training dataset.

ACKNOWLEDGEMENTS

Mahya Hajihassanpour and Georges Kesserwani were supported by the UK Engineering and Physical Sciences Research Council (EPSRC) grant EP/R007349/1. This work is part of the SEAMLESS-WAVE project (SoftwarE infrAstructure for Multi-purpose fLood modElling at variouS scaleS based on WAVElets (https://www.seamlesswave.com). The GPU-FV1 code is openly available on LISFLOOD-FP 8.0 with DOI: 10.5281/zenodo.4073011, with instructions on how to download, set-up and run the code available on: https://www.seamlesswave.com/LISFLOOD8.0. The codes to reproduce the analysis for the five UQ methods are openly available on: 10.5281/zenodo.7050213.

REFERENCES AND CITATIONS

[1] Abgrall, R., & Mishra, S. (2017). Uncertainty quantification for hyperbolic systems of conservation laws. *Handbook of Num. Anal.*, 507-544.

[2] Aitken, G., Beevers, L., & Christie, A. (2022). Multi-level Monte Carlo models for flood inundation uncertainty quantification. *Wat. Resour. Res.,* 58(11), 1-25.

[3] Alipour, A., Jafarzadegan, K., & Moradkhani, H. (2022), Global sensitivity analysis in hydrodynamic modeling and flood inundation mapping. *Env. Mod. & Soft.*, 152, 105398.

[4] Apel, H., Thieken, A. H., Merz, B., & Blöschl, G. (2004), Flood risk assessment and associated uncertainty. *Nat. Haz. Ear. Sys. Sci*, *4*(2), 295-308.

[5] Aronica, G., Hankin, B., & Beven, K. (1998), Uncertainty and equifinality in calibrating distributed roughness coefficients in a flood propagation model with limited data. *Adv. Wat. Resour.*, 22(4), 349-365.

[6] Avasarala, S., & Subramani, D. (2021), A non-Gaussian Bayesian filter for sequential data assimilation with non-intrusive polynomial chaos expansion. *Int. J. Numer. Meth. Eng.*, 122(23), 7156-7181.

[7] Bates, P. D., Pappenberger, F., & Romanowicz, R. J. (2011), Uncertainty in Flood Inundation Modelling, in Applied Uncertainty Analysis for Flood Risk Management. *Imperial College Press*, pp. 232-269.

[8] Beevers, L., Collet, L., Aitken, G., Maravat, C., & Visser, A. (2020), The influence of climate model uncertainty on fluvial flood hazard estimation, *Nat. Haz.* 104(3), 2489-2510.

[9] Bellos, V., & Tsihrintzis, V. (2021), Uncertainty aspects of 2D flood modelling in a benchmark case study. *17th International Conference on Environmental Science and Technology*, Athens, Greece.

[10] Bellos, V., Nalbantis, I., & Tsakiris, G. (2018), Friction Modeling of Flood Flow Simulations. *J. of Hydraul. Eng*. 144(12), 04018073.

[11] Botev, Z., & Ridder, A. (2017). *Variance Reduction*, Wiley StatsRef: Statistics Reference Online, pp. 1-6.

[12] Di Baldassarre, G., Schumann, G., Bates, P. D., Freer, J. E., & Beven, K. J. (2010), Flood-plain mapping: a critical discussion of deterministic and probabilistic approaches, *Hydrol.l Sci. J.* 55(3), 364-376.

[13] Dimitriadis, P., Tegos, A., Oikonomou, A., Pagana, V., Koukouvinos, A., Mamassis, N., Koutsoyiannis, D. & Efstratiadis, A. (2016). Comparative evaluation of 1D and quasi-2D hydraulic models based on benchmark and real-world applications for uncertainty assessment in flood mapping, *J. Hydrol.* 534, 478-492.

[14] Eldred, M. (2009). Recent Advances in Non-Intrusive Polynomial Chaos and Stochastic Collocation Methods for Uncertainty Analysis and Design, in 50th AIAA/ASME/ASCE/AHS/ASC Structures, Structural Dynamics, and Materials Conference, *American Institute of Aeronautics and Astronautics*.

[15] Etore, P., Fort, G., Jourdain, B. & Moulines, E. (2011). On adaptive stratification. *Annals of Operations Research*, 189(1), 127-154.

[16] Fan, Y. R., Huang, W. W., Li, Y. P., Huang, G. H. & Huang, K. (2015). A coupled ensemble filtering and probabilistic collocation approach for uncertainty quantification of hydrological models. *J. Hydrol.* 530, 255-272.

[17] Fewtrell, T. J., Neal, J. C., Bates, P. D. & Harrison, P. J. (2011). Geometric and structural river channel complexity and the prediction of urban inundation, *Hydrol. Processes*, 25(20), 3173-3186.

[18] Giunta, A. A., McFarland, J. M., Swiler, L. P. & Eldred M. S. (2006), The promise and peril of uncertainty quantification using response surface approximations, *Struct. & Infra. Eng.* 2(3-4), 175-189.

[19] Hajihassanpour, M., Kesserwani, G. Pettersson, P. & Bellos, V. (2023). Sampling-based methods for uncertainty propagation in flood modeling under multiple uncertain inputs: Finding out the most efficient choice. *Wat. Resour. Res.* 59(7), e2022WR034011.

[20] Hammersley, J. M. (1960). Monte Carlo methods for solving multivariable problems. *Annals of the New York Academy of Sciences*. 86(3), 844-874.

[21] Hu, P., Liu, X., & Hu, H. (2009). Accuracy assessment of digital elevation models based on approximation theory. *Photogrammetric Eng. & Remote Sensing*, 75(1), 49-56.

[22] Huang, Y., & Qin, X. (2014). Uncertainty analysis for flood inundation modelling with a random floodplain roughness field. *Environmental Sys. Res.* 3(1), 9.

[23] James, B. A. P. (1985). Variance reduction techniques, *J. Opera. Res. Soc.* 36(6), 525-530.

[24] Jung, Y., & Merwade, V. (2015). Estimation of uncertainty propagation in flood inundation mapping using a 1-D hydraulic model. *Hydrol. Proc.* 29(4), 624-640.

[25] Kalagnanam, J. R., & Diwekar, U. M. (1997). An efficient sampling technique for off-line quality control, *Technometrics*. 39(3), 308-319.

[26] Karamouz, M., & Fereshtehpour, M. (2019). Modeling DEM errors in coastal flood inundation and damages: A spatial nonstationary approach. *Wat. Resour. Res.* 55(8), 6606-6624.

[27] Kucherenko, S., Albrecht, D., & Saltelli, A. (2015). Exploring multi-dimensional spaces: A comparison of Latin hypercube and quasi Monte Carlo sampling techniques, *arXiv*, arXiv:1505.02350.

[28] Le Maître, O. P., Knio, O. M., Najm, H. N., & Ghanem, R. G. (2004). Uncertainty propagation using Wiener–Haar expansions. *J. Comput. Phys.* 197(1), 28-57.

[29] Liu, X, Hu, H., & Hu, P. (2015), Accuracy assessment of LiDAR-derived digital elevation models based on approximation theory. *Remote Sensing*. 7(6), 7062-7079.

[30] McKay, M. D., Beckman, R. J., & Conover, W. J. (1979). Comparison of three methods for selecting values of input variables in the analysis of output from a computer code. *Technometrics*, 21(2), 239-245.

[31] McMillan, H. K., & Brasington, J. (2008). End-to-end flood risk assessment: A coupled model cascade with uncertainty estimation. *Wat. Resour. Res.* 44(3), W03419, doi:10.1029/2007WR005995.

[32] Morokoff, W. J., & Caflisch, R. E. (1995). Quasi-Monte Carlo integration. *J. Comput. Phys.* 122(2), 218-230.

[33] Neal, J. C., Bates, P. D., Fewtrell, T. J., Hunter, N. M., Wilson, M. D., & Horritt, M. S. (2009). Distributed whole city water level measurements from the Carlisle 2005 urban flood event and comparison with hydraulic model simulations. *J. Hydrol.* 368(1), 42-55.

[34] Neelz, S., & Pender, G. (2013). Benchmarking the latest generation of 2D hydraulic modelling packages: Report - SC120002, *Environment Agency*.

[35] Nkwunonwo, U. C., Whitworth, M. & Baily B. (2020). A review of the current status of flood modelling for urban flood risk management in the developing countries. *Scientific African*. 7, e00269.

[36] Owen, A. B. (2013), Monte Carlo theory, methods and examples, *Art Owen*.

[37] Pettersson, & Krumscheid, S. (2022). Adaptive stratified sampling for nonsmooth problems. *Int. J. Uncertainty Quant.*, 12(6), 71-99.

[38] Pharr, M., Jakob, W. & Humphreys, G. (2016). Physically based rendering: From theory to implementation, *Morgan Kaufmann*.

[39] Rahman, A., Weinmann, P. E., Hoang, T. M. T., & Laurenson, E. M. (2002). Monte Carlo simulation of flood frequency curves from rainfall. *J. Hydrol.* 256(3), 196-210.

[40] Rubner, Y., Tomasi, C. & Guibas, L. J. (2000). The earth mover's distance as a metric for image retrieval. *Int. J. Computer Vision*. 40(2), 99-121.

[41] Shaw, J., & Kesserwani, G. (2020). Stochastic Galerkin finite volume shallow flow model: Well-balanced treatment over uncertain topography. *J. Hydraul. Eng.* 146(3), 04020005.

[42] Shaw, J., Kesserwani, G. & Pettersson, P. (2020). Probabilistic Godunov-type hydrodynamic modelling under multiple uncertainties: robust wavelet-based formulations, *Adv. Wat. Resour.* 137, 103526.

[43] Shields, M. D., Teferra, K., Hapij, A., & Daddazio, R. P. (2015). Refined stratified sampling for efficient Monte Carlo based uncertainty quantification. *Reliability Eng. & System Safety*, 142, 310-325.

[44] Shirvani, & M., G. Kesserwani (2021). Flood-pedestrian simulator for modelling human response dynamics during flood-induced evacuation: Hillsborough stadium case study. *Nat. Haz. Ear. Sys. Sci.* 21(10), 3175-3198.

[45] Shirvani, M. & Kesserwani, G., & Richmond, P. (2021). Agent-based simulator of dynamic flood-people interactions. *J. Flood Risk Manag.*14(2), e12695.

[46] Smemoe, C. M., Nelson, E. J., Zundel, A. K., & Miller, A. W. (2007). Demonstrating floodplain uncertainty using flood probability maps. *JAWRA J. American Wat. Resour. Assoc.* 43(2), 359-371.

[47] Stefanescu, E. R., Bursik, M., Cordoba, G., Dalbey, K., Jones, M. D., Patra, A. K., Pieri, D. C., Pitman, E. B., & Sheridan, M. F. (2012). Digital elevation model uncertainty and hazard analysis using a geophysical flow model, *Proc. Roy. Soc. A: Math., Phys. and Eng. Sci.* 468(2142), 1543-1563.

[48] Stephens, T. A., & Bledsoe, B. P. (2020). Probabilistic mapping of flood hazards: Depicting uncertainty in streamflow, land use, and geomorphic adjustment, *Anthropocene*, 29, 100231.

[49] Stricker, M.A., & Orengo, M. (1995). Similarity of color images, *Proc. SPIE 2420, Storage and Retrieval for Image and Video Databases III*.

[50] Wang, R., Diwekar, U., & Grégoire Padró, C. E. (2004). Efficient sampling techniques for uncertainties in risk analysis, *Env. Progress*. 23(2), 141-157.

[51] Wong, T. T., Luk, W. S., & Heng, P. A. (1997). Sampling with Hammersley and Halton Points, *J. Graph. Tools*. 2(2), 9-24.

[52] Xiu, D., & Karniadakis, G. E. (2002). The Wiener-Askey polynomial Chaos for stochastic differential equations. *SIAM J. Sci. Comput.* 24(2), 619-644.

[53] Zhang, J. (2021), Modern Monte Carlo methods for efficient uncertainty quantification and propagation: A survey, *WIREs Comput. Stat.* 13(5), e1539.

[54] Zhu, F., Zhong, P. A., Sun, Y. & Yeh, W. W. G. (2017). Real-time optimal flood control decision making and risk propagation under multiple uncertainties. *Wat. Resour. Res.* 53(12), 10635-10654.

[55] Zio, S., & Rochinha, F. A. (2012), A stochastic collocation approach for uncertainty quantification in hydraulic fracture numerical simulation. *Int. J. Uncertainty Quant.* 2(2), 145-160.

[56] Zokagoa, J. M., Soulaïmani, A., & Dupuis, P. (2021). Flood risk mapping using uncertainty propagation analysis on a peak discharge: case study of the Mille Iles River in Quebec. *Nat. Haz.* 107(1), 285-310.